# Increased rotational flow in the proximal aortic arch contributes to its dilation in bicuspid aortic valve disease

Lydia Dux-Santoy, MSc [a,†], José F. Rodríguez-Palomares, M.D, PhD [a,†], Andrea Guala, PhD [a], Gisela Teixidó-Turà, M.D, PhD [a], Aroa Ruiz-Muñoz, MSc [a], Giuliana Maldonado, M.D [a], Nicolás Villalva [a], Laura Galian, M.D [a], Filipa Valente, M.D. [a], Laura Gutiérrez, M.D [a], Teresa González-Alujas, M.D, PhD [a], Augusto Sao-Avilés PhD [a], Kevin M. Johnson, PhD [b], Oliver Wieben, PhD [b], David García-Dorado, M.D, PhD [a], Arturo Evangelista, M.D, PhD [a].

a. Hospital Universitari Vall d´Hebron, Department of Cardiology. Vall d'Hebron Institut de Recerca (VHIR). Universitat Autònoma de Barcelona. Barcelona. Spain.

b. Departments of Medical Physics & Radiology, University of Wisconsin – Madison, Madison, WI, USA

†. Both authors contributed equally to this study

**Funding**

This study has been partially funded by Beca Philips de la Societat Catalana de Cardiologia 2017.

**Address for correspondence:**

† José F Rodríguez-Palomares, M.D, PhD.

Department of Cardiology, Hospital Universitari Vall d´Hebron

Paseo Vall d'Hebron 119-129, 08035, Barcelona, Spain.

Phone: +3493 4893000; FAX: +3493 2746063

E-mail: jfrodriguezpalomares@gmail.com, jfrodrig@vhebron.net

# Abstract

**Aims**

Despite bicuspid aortic valve (BAV) aortopathy may extent to the proximal aortic arch, arch flow dynamics and its relation to dilation are still unexplored. Using 4D-flow MRI, we analyzed flow dynamics in the aortic arch per the BAV phenotype and its association with local dilation.

**Methods and results**

One hundred and eleven BAV patients (aortic diameters ≤ 55 mm, no severe valvular disease) and 45 age-matched tricuspid valve (TAV) (24 healthy volunteers, 21 with arch dilation) underwent 4D-flow. BAV were classified per fusion phenotype (83 RL, 28 RN) and arch dilation (48 non-dilated, 63 dilated). Peak velocity, jet angle, normalized displacement, in-plane rotational flow (IRF), wall shear stress, and systolic flow reversal ratio (SFRR) were calculated in 20 double-oblique planes along the thoracic aorta. ANCOVA and multivariable adjusted linear regression analysis were used to identify correlates of proximal arch dilation.

Arch dilation was present in 47% RL and 86% RN-BAV. Hypertension, aortic stenosis and male sex were associated with dilation in RL-BAV. BAV had higher rotational flow and eccentricity than TAV in the proximal arch. Dilated BAV compared to non-dilated had higher IRF, which was more pronounced in the RN-phenotype. RN-BAV, IRF and SFRR were independently associated with arch dilation. Flow parameters associated with dilation converged to the values found in healthy volunteers in the distal arch.

**Conclusion**

Increased rotational flow could justify dilation of the proximal arch in RN-BAV patients and in RL-BAV with male sex, hypertension and valvular stenosis. These patients may benefit from a closer follow-up with superior imaging techniques.


# Keywords

bicuspid aortic valve, 4D flow cardiovascular magnetic resonance (4D flow CMR), Aorta hemodynamics, aortic arch, Aortic dilation

# Introduction

Bicuspid aortic valve (BAV) is the most common cardiac congenital disease and is associated with a higher prevalence of aortic dilation than tricuspid aortic valve (TAV), with different dilation morphotypes associated with cusp fusion phenotypes (1). Patients with right-left (RL) cusp fusion usually present a dilation morphotype involving the aortic root and tubular ascending aorta (AscAo), while right-non coronary (RN) fusion has been related to tubular AscAo dilation and proximal aortic arch (proxArch) with no root dilation (1,2).

Proximal ascending aorta is the predominant area of dilation in BAV patients, thus, transthoracic echocardiography (TTE) is the main imaging technique for diagnosis, screening and clinical follow-up (3). However, BAV aortopathy may also involve the distal AscAo and proxArch, which are incompletely visualized by TTE or transesophageal echocardiography (blind spot). Thus, computed tomography (CT) or cardiac magnetic resonance (CMR) are needed to evaluate these aortic segments (3). Although both imaging techniques are indicated on current guidelines, the lack of ionizing radiation makes CMR preferable for patient follow-up (3).

Phase-contrast (PC) CMR allows quantification of aortic flow and, recently, 4D-flow sequences have enabled the evaluation of complex hemodynamics (4,5). This is of particular interest in BAV aortopathy since several studies have suggested that altered flow dynamics may contribute to AscAo dilation (6–11) beyond genetic causes (1,12), possibly through extracellular matrix dysregulation and elastic fiber degeneration (10). The influence of flow dynamics in aortic arch dilation has only been analyzed in few studies, which were always limited to basic metrics (6,13). A more detailed knowledge of arch flow dynamics in BAV may help identifying patients at higher risk of arch dilation, who may benefit from closer follow-up with other imaging techniques beyond echocardiography (CMR or CT).

Thus, using 4D-flow CMR, we aimed to analyze differences in the flow dynamic pattern in the aortic arch according to the valve phenotype in a large population of BAV patients and to establish its association with proxArch dilation. Also, we analyzed the relation between flow dynamics (from the sinotubular junction to the descending aorta at the diaphragm level) and the extension of BAV aortopathy.

# Methods

**Study population**

Patients with RL- or RN-phenotype, aortic root and AscAo diameters ≤ 55 mm and no severe valvular disease (aortic regurgitation ≤ III, aortic velocity < 3 m/s) by echo were consecutively and prospectively recruited. Inclusion criteria were: age > 18 years, sinus rhythm, no cardiovascular disease, uncontrolled arterial hypertension (HTA), connective tissue disorders, aortic coarctation or other congenital heart diseases and no contraindication for CMR. Age-matched TAV individuals were also included. The study was approved by the local ethics committee and informed consent was obtained from all participants.

**Cardiac-Magnetic Resonance protocol**

CMR studies were performed on a 1.5T Signa scanner (GE Healthcare, Waukesha, WI, USA). The protocol included 2D balanced steady-state free-precession (bSSFP) cine imaging to assess BAV phenotype and aortic diameters (using double-oblique multiplanar reconstruction), and 4D-flow acquisition with retrospective ECG-gating during free-breathing. Endovenous contrast was not given to minimize patient's risk.

A radially-undersampled acquisition (PC-VIPR) (14) with 5-point balanced velocity encoding (15) was used for 4D flow imaging of the entire thoracic aorta in 8-10 minutes total scan time. Acquisition parameters were: velocity encoding 200cm/s, field of view 400x400x400 $mm^3$, scan matrix 160x160x160, flip angle 8º, TR 4.2-6.4 ms and TE 1.9-3.7 ms. Reconstructions were performed offline to the nominal temporal resolution of each patient

(5xTR) with corrections for background phase from concomitant gradients and eddy currents, and trajectory errors of the 3D radial acquired k-space (14,15).

**Data analysis: 4D flow data processing**

The thoracic aorta was semi-automatically segmented from an angiogram derived from 4D-flow (4) and its centerline was computed using ITK-Snap (16). Co-registered 2D cine images were used to identify the sinotubular junction (STJ), the supra-aortic vessels and the diaphragmatic level. Based on these locations, equidistant analysis planes orthogonal to the centerline were distributed in three analysis regions: 8 planes in the AscAo (from the STJ to the brachiocephalic artery (BCA)), 4 in the arch (from the BCA to the left subclavian artery) and 8 in the thoracic descending aorta (DescAo) (from the left subclavian artery to the diaphragmatic level). A reference point corresponding to the inner curvature of the aorta was defined on every contour to allow spatial registration between patients. For each plane, 3D velocity data were exported for calculations to be made using in-house code developed in Matlab (MathWorks Inc, Natick, MA, USA). Peak-systolic parameters were averaged using 1 time-frame before and 2 time-frames after peak systole to mitigate noise (17).

Detailed analysis of flow in the aortic arch and its relation to proxArch dilation was assessed. Additionally, flow parameters distribution along the thoracic aorta (from the STJ to the diaphragm) was analyzed to explore the relation between flow alterations and the extension of BAV aortic dilation.

**Flow parameters**

Peak velocity magnitude, flow eccentricity (jet angle and displacement) and in-plane rotational flow (IRF) were calculated for each analysis plane.

Flow eccentricity was obtained as described by Sigovan et al. (18). IRF was quantified as the through-plane component of circulation, which is used in fluid dynamics to quantify rotation of flow within a plane (8). The sign of IRF indicates the sense of flow rotation (right-

handed/anti-clockwise for positive IRF, left-handed/clockwise for negative IRF). Normal IRF values were defined by healthy volunteers (HV) (mean ± 2SD). Systolic flow reversal ratio (SFRR) was calculated as the ratio of backward to forward flow volume in systole (19).

**Wall shear stress**

Peak-systolic vectorial wall shear stress (WSS) was calculated by fitting the 3D velocity data with B-spline surfaces and computing velocity derivatives on 64 points equally distributed on the segmented vessel contour (20). Contour-averaged magnitude ($WSS_{mag,avg}$), axial ($WSS_{ax,avg}$) and circumferential WSS ($WSS_{circ,avg}$) were obtained.

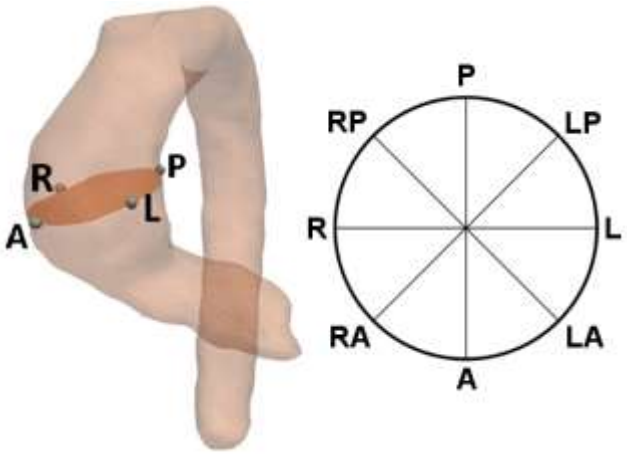


*Figure 1. Regional WSS measurement regions. A: anterior, L: left, P: Posterior, R: right.*

WSS maps were obtained for every plane once discretized in 8 circumferential regions (anterior/left-anterior/left/left-posterior/posterior/right-posterior/right/right-anterior) defined using the inner reference point (Figure 1). Using these values, point-to-point averaged WSS and p-value were obtained for each BAV phenotype and dilation, and used to visualize regional maps. To better understanding of WSS maps, the distal AAo was also represented in regional maps.

**Aortic arch dilation**

The aortic diameter was automatically measured at the BCA level over the segmented aorta**.** To determine the presence of arch dilation the expected normal diameter proximal to the

BCA was calculated on the basis of the age for each patient using the regression formulas by Hager et al (21). Arch dilation was considered when the measured diameter was greater than the expected diameter.

**Statistical analysis**

Continuous variables were expressed as mean ± standard deviation and assessed for normality using the Shapiro-Wilk test. Continuous variables were compared using Student's t-test if they presented a normal distribution, and Mann-Whitney U test if they did not present a normal distribution. Categorical variables were analyzed with the chi-square test.

Multivariable linear regression analysis with a backward selection procedure was used to evaluate relations between demographic and flow variables and proxArch dilation. Variables were entered into the model if $P < 0.25$ (22) in univariate analyses.

A two-tailed P-value $< 0.05$ was considered statistically significant. SPSS 19.0 (IBM SPSS Statistics, Chicago, Illinois, USA) was used for the analysis.

# Results

One hundred and eleven BAV patients (83 RL- and 28 RN-phenotype) and 45 age-matched TAV (24 HV and 21 with proxArch dilation) completed the study protocol. Demographic characteristics and aortic diameters among groups are shown in Table 1. BAV presented larger aortic diameters than TAV both in the sinus of Valsalva (SoV) ($p=0.044$) and AscAo ($p=0.004$), higher diastolic arterial pressure ($p<0.001$) and higher prevalence of (non-severe) aortic valve disease ($p<0.001$ for regurgitation and $p=0.004$ for stenosis).

Arch dilation was present in 56.8% BAV, with a prevalence of 46.9% in RL-BAV and 85.7% in RN-BAV ($p<0.001$). Aortic arch dilated RL-BAV compared to non-dilated RL presented higher prevalence of male sex (79.5% vs 50.0%, $p=0.005$), mild-to-moderate stenosis

(38.5% vs 18.2%, p=0.039) and HTA (42.3% vs 29.7%, p=0.003). No differences between dilated and non-dilated BAV were obtained when analyzing additional clinical variables.

## Flow dynamics in the aortic arch

Table 2 and Table 3 summarize results of flow analysis in the proximal and distal (distArch) arch, which are the first and last analysis plane located in the aortic arch. Results with the analysis in all slices are shown in Table S1 and Table S2.

### Aortic arch flow dynamics and BAV phenotype

Flow rotation along the arch was right-handed in most HV (87.5%) and BAV (94.6%), both for RL and RN phenotypes. Abnormally increased right-handed rotational flow (>84.6 $cm^2/s$, defined by HV controls mean + 2SD) was present in 21.6% RL-BAV and in 57.2% RN-BAV, and in only one HV (4.2%).

Compared to HV, BAV patients with non-dilated arch presented higher IRF ($p<0.05$) in the proxArch and larger normalized displacement ($p<0.05$) in the proximal and mid arch. All variables were similar between both groups in the distArch except normalized displacement ($p<0.05$).

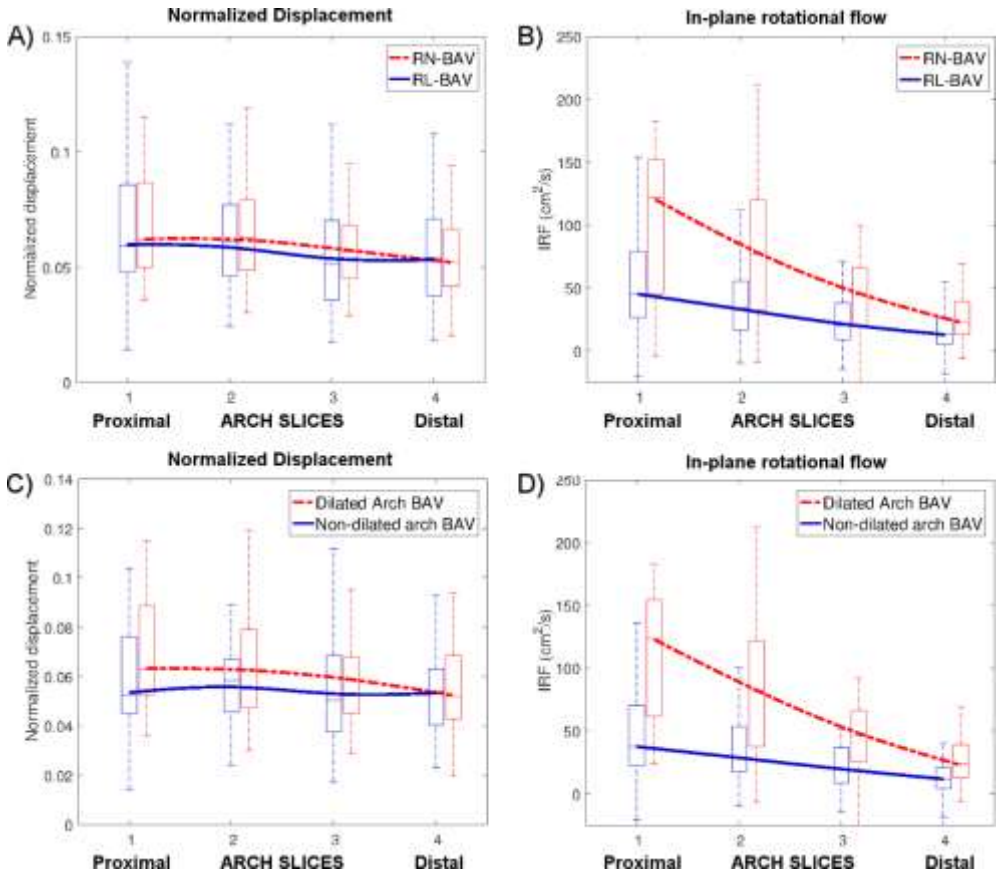


*Figure 2. Normalized displacement and in-plane rotational flow in BAV per BAV phenotype (a, b) and arch dilation (c, d).*

Patients with RN-BAV compared to RL-BAV presented significantly higher rotational flow (IRF) (Figure 2b) and $WSS_{circ,avg}$ at all arch levels ($p<0.001$ for IRF and $WSS_{circ,avg}$ at proxArch; $p=0.013$ for IRF at distArch), but similar flow displacement (Figure 2a, Table 2 and Table S1).

Regional axial WSS map was similar in both BAV phenotypes (Figure 3a), while circumferential WSS was significantly higher in RN-BAV in all aortic segments in distal AscAo and proxArch (Figure 3).

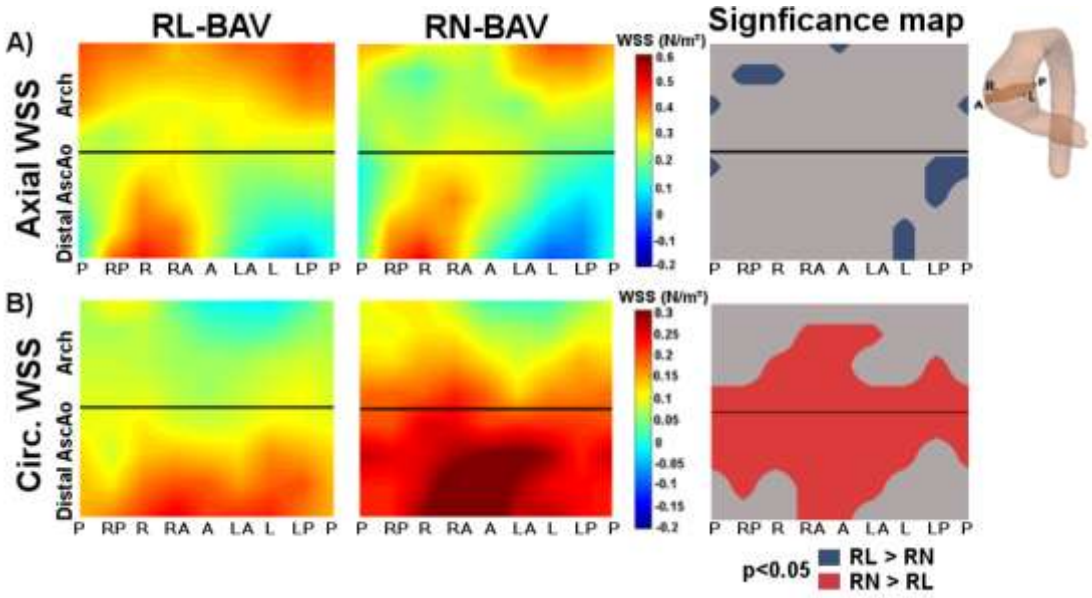


*Figure 3. Regional WSS maps in the different BAV phenotypes and statistically- significant difference (p<0.05). A) Axial WSS shows minimum differences. B) Circumferential WSS is higher in RN-BAV at mid-distal ascending aorta and proximal-mid arch.*

**Aortic arch flow dynamics and arch dilation in BAV and TAV**

Dilated TAV compared to HV presented similar normalized displacement and rotational flow, while higher SFRR and lower $WSS_{ax,avg}$ along the arch were noted (Table 3 and Table S2).

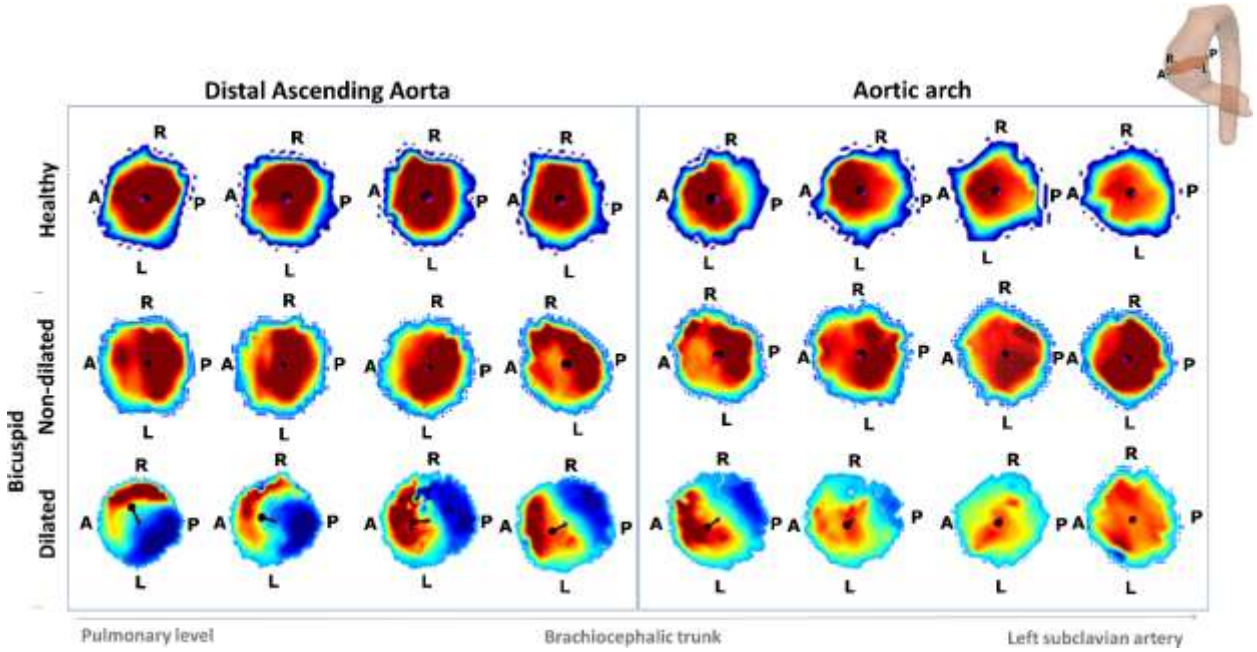


*Figure 4. Flow displacement at the distal ascending aorta and aortic arch in a healthy volunteer and in BAV with non-dilated and dilated arch. Dilated BAV presents increased displacement.*

When comparing BAV according to arch dilation, dilated BAV had greater IRF and SFRR than non-dilated at all levels of the arch (Figure 2d and Figure 6), increased normalized displacement (Figure 2c, Figure 4 and Figure 6) and lower $WSS_{ax,avg}$ at the proxArch (Table 3 and Table S2). Similar findings were observed in dilated RL-BAV compared to non-dilated RL (Table 2 and Table S1), and in dilated RN-BAV compared to non-dilated RN. However, the reduced number of non-dilated RN did not allow for statistical comparison.

Regional axial WSS (WSS maps) was decreased in dilated BAV (figure 5a), while regional circumferential WSS was increased in dilated BAV in the anterior wall at proximal-mid aortic arch (figure 5b).

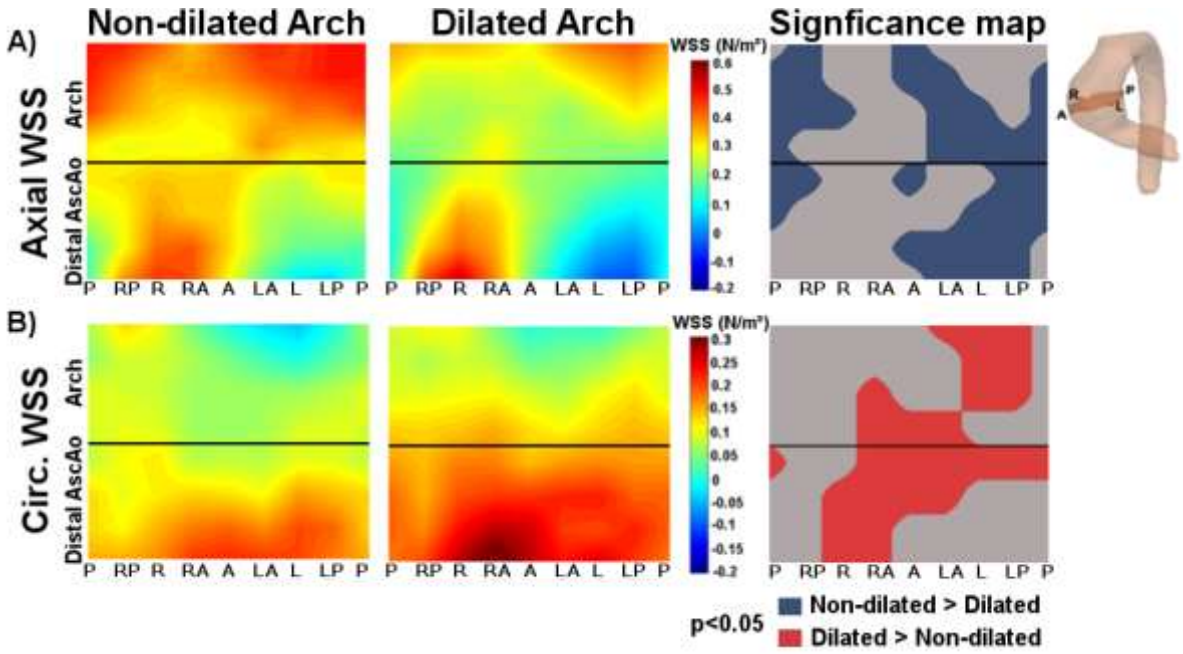


*Figure 5. Regional WSS maps in BAV patients with dilated and non-dilated arch and statistically-significant difference (p<0.05). A) Axial WSS is regionally reduced in presence of dilation. B) Circumferential WSS is increased in dilated BAV in anterior wall at proximal-mid arch.*

In order to analyze if differences in flow in the aortic arch were a consequence of dilation or may play a causal role, dilated BAV were compared with age and size-matched arch-dilated TAV. This analysis showed that dilated BAV compared to dilated TAV still presented larger normalized displacement ($p<0.001$) and higher rotational flow in the proximal and mid arch ($p<0.001$ proxArch, $p<0.05$ mid arch for IRF and $WSS_{circ,avg}$) (Table 3 and Table S2).

**Multivariable correlated of proximal arch dilation in BAV**

Significant unadjusted and multivariable adjusted correlates of proxArch dilation in BAV are listed in Table 4. Significant unadjusted correlates of proxArch dilation were BAV phenotype (RN-BAV), sex, body height and weight, in addition to increased rotational flow (IRF and SFRR). On multivariable analysis RN-BAV, body height, IRF and SFRR were independently related to arch dilation.

In addition, we performed the multivariate analysis considering the aortic arch diameter (as a continuous variable) and with the same clinical and flow variables (Table 5). This analysis also confirmed the independent relations between arch diameter and rotational flow parameters (IRF $p=0.008$ and SFRR $p=0.007$) as well as BAV phenotype (RN-BAV), ($p=0.018$).

**Flow distribution in the thoracic aorta**

To understand why aortic dilation mainly involves the AscAo extending to the proxArch, we compared flow parameters distribution along the thoracic aorta (ascending, arch and descending until the level of the diaphragm) for non-dilated and dilated arch BAV and HV (Figure 6).

Compared to HV, BAV presented increased rotational flow, eccentricity and SFRR in the AscAo, extending to the proxArch. These parameters were particularly increased in dilated compared to non-dilated BAV. In BAV, flow eccentricity (jet angle and displacement),

rotational flow (IRF and $WSS_{circ,avg}$) and SFRR presented their highest values in the AscAo region, reaching its maximum at mid AscAo. These parameters decreased afterwards, converging along the mid-distal arch and proximal DescAo and approximating to values in HV (Figure 6 and Table S1).

A change in direction of flow rotation in the DescAo was observed in both BAV and HV, from right-handed flow in the AscAo and arch (positive $WSS_{circ,avg}$ or IRF) to left-handed in the DescAo (negative $WSS_{circ,avg}$ or IRF) (Figure 6).

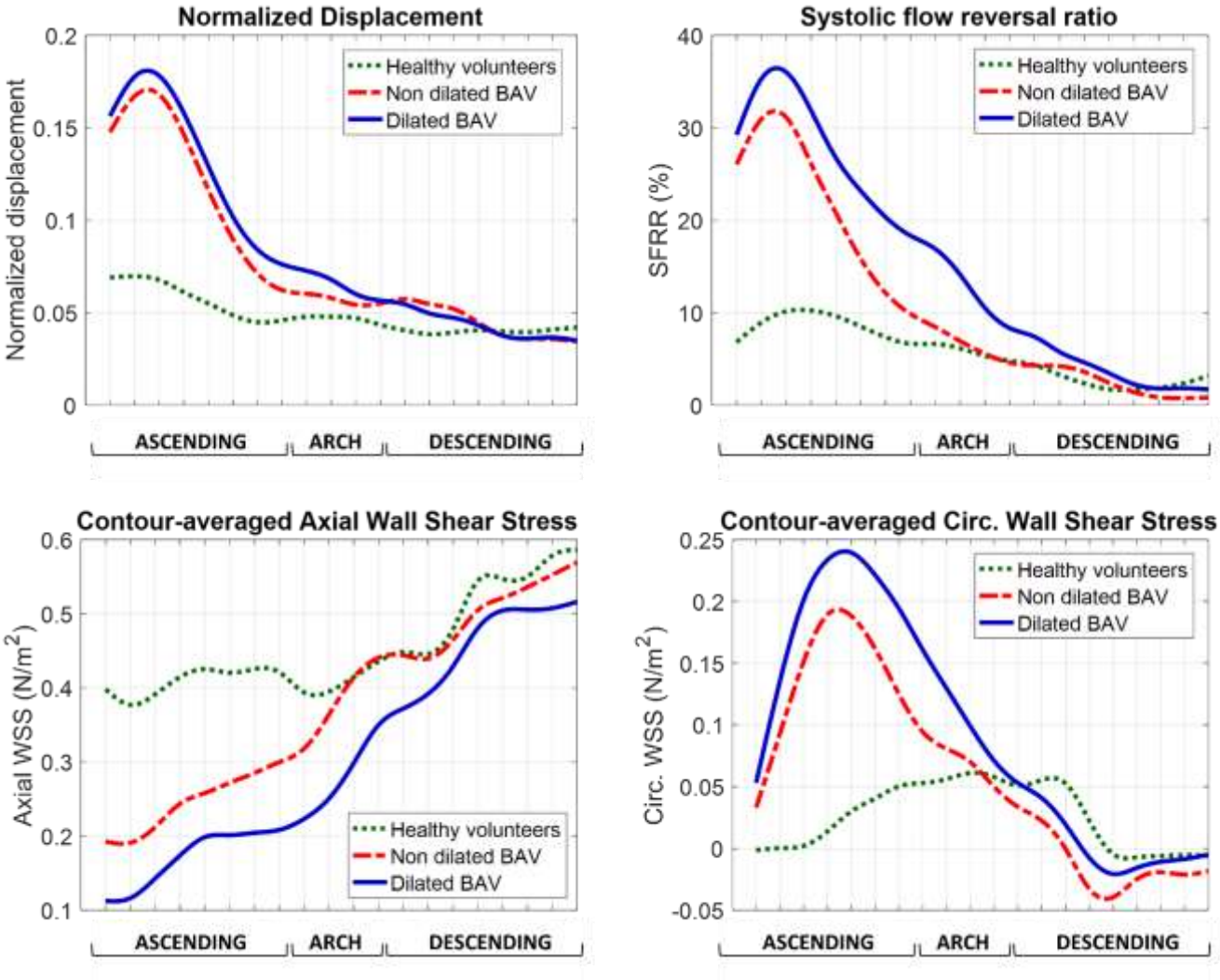


*Figure 6. Flow parameters along the thoracic aorta in HV and BAV with non-dilated and dilated arch, showing differences in the ascending aorta and the proximal arch. Dilated BAV presented higher displacement, systolic flow reversal ratio and contour-averaged WSS than non-dilated, but reduced axial WSS.*

# Discussion

In the present study, we analyzed complex flow variables and vectorial WSS along the arch and their association with aortic arch dilation in a large BAV population without severe valvulopathy. Clinical information about flow in the aortic arch is scarce, hence, the relevance of our work and our findings.

The main findings of this study are:

1) BAV patients with proximal arch dilation have increased rotational flow (IRF and $WSS_{circ,avg}$) with respect to the non-dilated, which is more pronounced in the RN-BAV phenotype (86%). However, 47% of RL-BAV also presented arch dilation. These patients presented higher rates of hypertension, aortic stenosis and male sex than non-dilated. Also, BAV have higher rotational flow and greater eccentricity than HV and dilated TAV patients.
2) The factors independently associated with proxArch dilation are valvular phenotype (RN) and rotational flow parameters (IRF and SFRR).
3) Flow parameters associated with dilation differ between dilated and non-dilated BAV at the AscAo and the proxArch (greater in dilated BAV), and converged to values in HV along the distArch and the DescAo.

Previous studies have reported that altered flow dynamics in the AscAo in BAV may contribute to its dilation (6,8,11,23), possibly through the degradation of the extracellular matrix and elastic fibers (10). To our knowledge this is the first study conducted in a large BAV population in which the persistence of altered flow dynamics in the proxArch has been reported and related to local dilation, identifying which patients may be at a major risk of arch dilation and may benefit from closer follow-up.

**Aortic arch measurements**

Most studies defining normality values for thoracic aorta diameters do not assess the aortic arch (3). Only few studies have provided reference values for the aortic arch diameter in the pediatric population (24) and in adults (21,25,26), using different anatomical landmarks and imaging techniques. Consequently, there is no agreement in the definition of aortic arch dilation and predefined cut-off points are generally used (30 or 40 mm) (6,9). Instead of using a predefined cut-off, we used an age-dependent threshold for proxArch dilation based on the regression formulas of Hager et al. (21) which is, to our knowledge, the only work that provides a normality value for proxArch diameter in adults (at the level of the BCA) based on CT. However, it presents the limitation that it does not consider the diameter dependence with body dimension or sex demonstrated in other studies (25,26).

In our population, proxArch dilation was present in 56.8% of BAV, mainly affecting the RN-BAV (86% dilated vs 47.0% in the RL-BAV) as previously reported (9,12,27). Other studies have reported different prevalence of arch dilation in BAV, with dilated arch in 23.4%-73% in general BAV population (9,27), 7-13% in RL-BAV and 34.0-40.5% in RN-BAV (2,6,9). However, the use of different imaging techniques (echocardiography, CT or angiography derived from 4D-flow) and predefined cut-off points in these studies could explain this variability.

**Aortic arch flow dynamics in BAV**

Previous studies have reported the existence of eccentric (6,8,11,23) and increased rotational flow (8,28–30) in the AscAo in BAV patients compared to tricuspid, leading to an increased aortic WSS with asymmetric regional distribution (8,10,17,29,30). In our study, we observed that increased flow eccentricity (normalized displacement) and rotational flow (IRF

and $WSS_{circ,avg}$) were still different in the proximal and mid arch when comparing BAV and TAV patients, while other parameters (maximum velocity, SFRR, $WSS_{ax,avg}$) were similar.

This increased rotational flow was particularly high in the RN-phenotype (coinciding with a higher rate of arch dilation), as previously reported in the AscAo (8), generating an increased circumferential WSS in all segments of the proxArch. However, the differences in flow displacement between BAV phenotypes reported in the AscAo (6) were not present in the proxArch, indicating they have similar velocity profiles at this level (31).

**Determinants of aortic arch dilation in BAV**

We did not find a difference between BAV with dilated and non-dilated arch in relation to the presence of raphe, valve calcification or HTA, as reported by Kang et al. (9). However, in the RL-BAV, arch dilation was associated with the presence of stenosis and HTA, which have been previously related to AscAo dilation (9,32), and to the male sex, which has been previously related to root dilation (2).

BAV patients with proxArch dilation (mostly RN-BAV) presented increased rotational flow in the proxArch, as occurs in the AscAo (8,31). However, this increased rotational flow was not observed when comparing dilated TAV and HV, suggesting it is not a consequence of dilation but it is associated with the BAV and may play a causal role, as suggested elsewhere (8,31). Moreover, this rotational flow leads to an asymmetrically increased circumferential WSS in the proxArch of dilated BAV, which may contribute to aortic wall degradation and dilation as described in the AscAo (10).

Furthermore, dilated BAV compared to non-dilated showed a larger normalized displacement in the proxArch, although differences were smaller than in rotational flow, indicating that increased eccentricity may also contribute to dilation as occurs in the AscAo (6,23,31). Although lower $WSS_{ax,avg}$ and higher SFRR were present in BAV patients with dilated arch, they were also observed in dilated TAV compared to HV and may be a

consequence of dilation (33). However, systolic retrograde flow has also been suggested as an early marker of aortic remodeling (19).

The independent association of vortical flow parameters (both in-plane IRF and through-plane SFRR) together with valvular phenotype (RN) with proxArch dilation in BAV was confirmed in the multivariable analysis.

**Aortic flow and BAV aortopathy**

We reported predominantly right-handed rotational flow in the AscAo and arch in BAV patients and HV, changing to left-handed rotation in the DescAo. This behaviour has been previously reported in healthy subjects (20,34,35), attributing the change in direction of rotation in the DescAo to the distal arch curvature (34).

The distribution of flow parameters along the thoracic aorta revealed that differences in flow variables associated to dilation exist not only in the AscAo but also in the proxArch, which are the regions mainly affected in BAV aortopathy (1), but converged to values in HV in the regions respected by the dilation (distArch and DescAo). This result supports the role of flow in aortic dilation and may justify that the geometric alterations in BAV mainly affect the AscAo and the proxArch.

**Imaging follow-up**

Diagnosis, screening and follow-up of BAV patients is based on TTE imaging (3). However, this imaging technique does not allow the evaluation of the distal AscAo and proxArch, regions that may also present local flow alterations that may contribute to its dilation. Thus, a more complete evaluation of the AscAo and the proximal-mid arch with advanced imaging techniques (such as CMR or CT), including local flow evaluation, could of benefit for those patients at a major risk of arch dilation. Therefore, our study shows that RN-BAV patients, patients with increased rotational flow and RL-BAV patients with male sex, HTA and valvular stenosis may benefit from a closer follow-up.

**Limitations**

We conducted a cross-sectional study to evaluate the correlation between flow dynamics and aortic arch dilation in BAV. However, the eventual causal role of these parameters on the development of arch dilation needs to be determined in further longitudinal studies.

Arch dilation was defined using an age-dependent diameter threshold for dilation, but did not account for diameter dependence with BSA and sex (25,26). However, this definition is based on the only study providing reference values for proximal arch diameter (21), and it is superior to the use of predefine diameter thresholds (6,9).

Regional WSS maps are affected by several methodological limitations: the supra-aortic trunks were not considered in the segmentation, and maps were estimated by interpolating values on a relatively limited number of analysis planes. Additionally, WSS is known to be underestimated because of the limited spatial and temporal resolution of 4D flow (5,20,36). However, as all acquisitions were made using the same imaging parameters and analyzed with the same methodology, comparison between groups is unbiased. Additionally, the robustness of WSS measurements employed in this study and their reproducibility has been previously demonstrated (37). Also, flow analysis was limited to peak systole, averaging the results obtained at four successive time phases to reduce noise. Despite this approach may imply the loss of temporal information, it has been used in other studies (6,8,29) and it is high reproducible (38).

# Conclusions

BAV patients with proximal arch dilation present greater rotational flow than non-dilated, being more marked in RN-BAV and in RL-BAV patients with male sex, HTA and

significant valvular stenosis. This rotational flow could justify proximal arch dilation in this population. Thus, these patients may benefit from a closer follow-up with CMR or CT.

In addition, our study shows that the flow variables associated with dilation present differences in the ascending aorta and the proximal arch, which are the regions mainly affected in bicuspid aortopathy, but converge in the regions not affected by the dilation (distal arch and descending aorta). This result supports the role of altered flow dynamics in BAV aortopathy.

# Supplementary data

**Table S1**. Flow dynamics along the aortic arch (proximal to distal slices) in bicuspid aortic valve phenotypes per arch dilation.

**Table S2.** Table S2. Flow dynamics along the aortic arch (proximal to distal slices) in bicuspid aortic valve and age-matched tricuspid valve subjects per arch dilation.

# Acknowledgements

We would like to thank Christopher François (University of Wisconsin-Madison) and Rob van der Geest (Leiden University Medical Center) for advice on 4D-flow sequences, and Roberto García Álvarez (GE Healthcare) for technical support. We are also grateful to Christine O'Hara for English revisions.

# References

1. Verma S, Siu SC. Aortic Dilatation in Patients with Bicuspid Aortic Valve. N Engl J Med. 2014;370(20):1920–9.
2. Della Corte A, Bancone C, Dialetto G, Covino FE, Manduca S, Montibello M V., et al. The ascending aorta with bicuspid aortic valve: a phenotypic classification with potential prognostic significance. Eur J Cardiothorac Surg. 2014;46:240–7.
3. Erbel RA, Aboyans V, Boileau C, Bossone E, Di Bartolomeo R, Eggebrecht H, et al. 2014 ESC guidelines on the diagnosis and treatment of aortic diseases. Eur Heart J. 2014;35(41):2873–926.
4. Markl M, Frydrychowicz A, Kozerke S, Hope MD, Wieben O. 4D flow MRI. J Magn Reson Imaging. 2012;36(5):1015–36.
5. Dyverfeldt P, Bissell MM, Barker AJ, Bolger AF, Carlhäll C-J, Ebbers T, et al. 4D

flow cardiovascular magnetic resonance consensus statement. J Cardiovasc Magn Reson. 2015;17:72.

6. Mahadevia R, Barker AJ, Schnell S, Entezari P, Kansal P, Fedak PWMM, et al. Bicuspid aortic cusp fusion morphology alters aortic three-dimensional outflow patterns, wall shear stress, and expression of aortopathy. Circulation. 2014;129:673–82.
7. Hope MD, Hope TA, Meadows AK, Ordovas KG, Urbania TH, Alley MT, et al. Bicuspid aortic valve: four-dimensional MR evaluation of ascending aortic systolic flow patterns. Radiology. 2010;255(1):53–61.
8. Bissell MM, Hess AT, Biasiolli L, Glaze SJ, Loudon M, Pitcher A, et al. Aortic dilation in bicuspid aortic valve disease: Flow pattern is a major contributor and differs with valve fusion type. Circ Cardiovasc Imaging. 2013;6(4):499–507.
9. Kang JW, Song HG, Yang DH, Baek S, Kim DH, Song JM, et al. Association between bicuspid aortic valve phenotype and patterns of valvular dysfunction and bicuspid aortopathy: Comprehensive evaluation using MDCT and echocardiography. JACC Cardiovasc Imaging. 2013;6:150–61.
10. Guzzardi DG, Barker AJ, Van Ooij P, Malaisrie SC, Puthumana JJ, Belke DD, et al. Valve-Related Hemodynamics Mediate Human Bicuspid Aortopathy: Insights From Wall Shear Stress Mapping. J Am Coll Cardiol. 2015;66(8):892–900.
11. Burris NS, Sigovan M, Knauer HA, Tseng EE, Saloner D, Hope MD. Systolic flow displacement correlates with future ascending aortic growth in patients with bicuspid aortic valves undergoing magnetic resonance surveillance. Invest Radiol. 2014;49(10):635–9.
12. Girdauskas E, Borger MA, Secknus MA, Girdauskas G, Kuntze T. Is aortopathy in bicuspid aortic valve disease a congenital defect or a result of abnormal

hemodynamics? A critical reappraisal of a one-sided argument. Eur J Cardiothorac Surg. 2011;39:809–14.

13. Raghav V, Barker AJ, Mangiameli D, Mirabella L, Markl M, Yoganathan AP. Valve mediated hemodynamics and their association with distal ascending aortic diameter in bicuspid aortic valve subjects. J Magn Reson Imaging. 2017;0:0–0.
14. Johnson KM, Lum DP, Turski PA, Block WF, Mistretta CA, Wieben O. Improved 3D Phase Contrast MRI with Off-resonance Corrected Dual Echo VIPR. Magn Reson Med. 2008;60(6):1329–36.
15. Johnson KM, Markl M. Improved SNR in phase contrast velocimetry with five-point balanced flow encoding. Magn Reson Med. 2010;63(2):349–55.
16. Yushkevich PA, Piven J, Hazlett HC, Smith RG, Ho S, Gee JC, et al. User-guided 3D active contour segmentation of anatomical structures: Significantly improved efficiency and reliability. Neuroimage. 2006;31(3):1116–28.
17. Barker AJ, Markl M, Bürk J, Lorenz R, Bock J, Bauer S, et al. Bicuspid aortic valve is associated with altered wall shear stress in the ascending aorta. Circ Cardiovasc Imaging. 2012;5(4):457–66.
18. Sigovan M, Hope MD, Dyverfeldt P, Saloner D. Comparison of four-dimensional flow parameters for quantification of flow eccentricity in the ascending aorta. J Magn Reson Imaging. 2011;34(5):1226–30.
19. Bensalah MZ, Bollache E, Kachenoura N, Giron A, De Cesare A, Macron L, et al. Geometry is a major determinant of flow reversal in proximal aorta. Am J Physiol Heart Circ Physiol. 2014;306(10):H1408-16.
20. Stalder AF, Russe MF, Frydrychowicz A, Bock J, Hennig J, Markl M. Quantitative 2D and 3D phase contrast MRI: Optimized analysis of blood flow and vessel wall parameters. Magn Reson Med. 2008;60(5):1218–31.

21. Hager A, Kaemmerer H, Rapp-Bernhardt U, Blücher S, Rapp K, Bernhardt TM, et al. Diameters of the thoracic aorta throughout life as measured with helical computed tomography. J Thorac Cardiovasc Surg. 2002;123(6):1060–6.

22. Mickey RM, Greenland S. The impact of confounder selection criteria on effect estimation. Am J Epidemiol. 1989;129(1):125–37.

23. den Reijer PM, Sallee III D, van der Velden P, Zaaijer ER, Parks WJ, Ramamurthy S, et al. Hemodynamic predictors of aortic dilatation in bicuspid aortic valve by velocity-encoded cardiovascular magnetic resonance. J Cardiovasc Magn Reson. 2010;12:4.

24. Kaiser T, Kellenberger CJ, Albisetti M, Bergsträsser E, Valsangiacomo Buechel ER. Normal values for aortic diameters in children and adolescents--assessment in vivo by contrast-enhanced CMR-angiography. J Cardiovasc Magn Reson. 2008;10:56.

25. Agmon Y, Khandheria BK, Meissner I, Schwartz GL, Sicks JD, Fought AJ, et al. Is aortic dilatation an atherosclerosis-related process? Clinical, laboratory, and transesophageal echocardiographic correlates of thoracic aortic dimensions in the population with implications for thoracic aortic aneurysm formation. J Am Coll Cardiol. 2003;42(6):1076–83.

26. Mirea O, Maffessanti F, Gripari P, Tamborini G, Muratori M, Fusini L, et al. Effects of aging and body size on proximal and ascending aorta and aortic arch: Inner edge-to-inner edge reference values in a large adult population by two-dimensional transthoracic echocardiography. J Am Soc Echocardiogr. 2013;26(4):419–27.

27. Fazel SS, Mallidi HR, Lee RS, Sheehan MP, Liang D, Fleischman D, et al. The aortopathy of bicuspid aortic valve disease has distinctive patterns and usually involves the transverse aortic arch. J Thorac Cardiovasc Surg. 2008;135(4).

28. Kolipaka A, Illapani VSP, Kalra P, Garcia J, Mo X, Markl M, et al. Quantification and comparison of 4D-flow MRI-derived wall shear stress and MRE-derived wall stiffness

of the abdominal aorta. J Magn Reson Imaging. 2016;

29. Meierhofer C, Schneider EP, Lyko C, Hutter A, Martinoff S, Markl M, et al. Wall shear stress and flow patterns in the ascending aorta in patients with bicuspid aortic valves differ significantly from tricuspid aortic valves: a prospective study. Eur Heart J Cardiovasc Imaging. 2013;14(8):797–804.
30. Hope MD, Hope TA, Crook SES, Ordovas KG, Urbania TH, Alley MT, et al. 4D flow CMR in assessment of valve-related ascending aortic disease. JACC Cardiovasc Imaging. 2011;4(7):781–7.
31. Rodríguez-Palomares JF, Dux-Santoy L, Guala A, Kale R, Maldonado G, Teixidó-Turà G, et al. Aortic flow patterns and wall shear stress maps by 4D-flow cardiovascular magnetic resonance in the assessment of aortic dilatation in bicuspid aortic valve disease. J Cardiovasc Magn Reson. 2018;20(1):28.
32. Della Corte A, Bancone C, Quarto C, Dialetto G, Covino FE, Scardone M, et al. Predictors of ascending aortic dilatation with bicuspid aortic valve: a wide spectrum of disease expression. Eur J Cardiothorac Surg. 2007;31(3):397–405.
33. Burk J, Blanke P, Stankovic Z, Barker AJ, Russe M, Geiger J, et al. Evaluation of 3D blood flow patterns and wall shear stress in the normal and dilated thoracic aorta using flow-sensitive 4D CMR. J Cardiovasc Magn Reson. 2012;14(1):84.
34. Kilner PJ, Yang GZ, Mohiaddin RH, Firmin DN, Longmore DB. Helical and retrograde secondary flow patterns in the aortic arch studied by three-directional magnetic resonance velocity mapping. Circulation. 1993;88(part 1):2235–47.
35. Bogren HG, Buonocore MH. 4D Magnetic Resonance Velocity Mapping of Blood Flow Patterns in the Aorta in Young vs. Elderly Normal Subjects. J Magn Reson Imaging. 1999;10:861–9.
36. Cibis M, Potters W V, Gijsen FJ, Marquering H, Van Ooij P, Van Bavel E, et al. The

effect of spatial and temporal resolution of cine phase contrast MRI on wall shear stress and oscillatory shear index assessment. PLoS One. 2016/09/27. 2016;11(9):e0163316.

37. Markl M, Wallis W, Harloff A. Reproducibility of flow and wall shear stress analysis using flow-sensitive four-dimensional MRI. J Magn Reson Imaging. 2011/03/31. 2011;33(4):988–94.

38. Van Ooij P, Powell AL, Potters W V, Carr JC, Markl M, Barker AJ. Reproducibility and interobserver variability of systolic blood flow velocity and 3D wall shear stress derived from 4D flow MRI in the healthy aorta. J Magn Reson Imaging. 2015/07/04. 2016;43(1):236–48.

# Tables

*Table 1. Demographics in TAV and BAV. Statistical significance (p<0.05) comparing: * TAV vs BAV counterpart, †dilated vs non-dilated counterpart.*

| | TAV | | | BAV | | |
|---|---|---|---|---|---|---|
| | **ALL (n=45)** | **Healthy (n=24)** | **Dilated (n=21)** | **ALL (n=111)** | **Non-dilated (n=48)** | **Dilated (n=63)** |
| **Age (years)** | 48.0±16.0 | 44.8±17.1 | 51.7±14.1 | 50.9±13.9 | 50.3±14.0 | 51.4±14.0 |
| **Men (%)** | 66.7 | 62.5 | 71.4 | 64 | 50 | 74.6† |
| **Weight (kg)** | 73.6±11.3 | 72.2±10.9 | 75.0±11.8 | 75.3±13.1 | 70.2±13.2 | 79.3±11.6† |
| **Height (cm)** | 170.2±9.4 | 168.5±9.5 | 172.0±9.3 | 170.8±9.7 | 167.3±10.9 | 173.4±7.7† |
| **BSA ($m^2$)** | 1.85±0.17 | 1.81±0.16 | 1.88±0.18 | 1.87±0.20 | 1.79±0.21 | 1.93±0.16† |
| **RL-BAV/RN-BAV** | - | - | - | 83/28 | 44/4 | 39/24† |
| **Raphe (%)** | - | - | - | 68.8 | 68.8 | 68.9 |
| **Calcification (%)** | - | - | - | 48.8 | 45.9 | 51.0 |
| **Hypertension (%)** | 46.6 | 0.0 | 100 † | 37.1 | 29.7 | 42.3 |
| **Smoking (%)** | 24.4 | 20.8 | 33.3 | 9.2 | 8.1 | 10.0 |
| **Diabetes (%)** | 15.5 | 0.0 | 33.3 | 6.9 | 8.1 | 6.0 |
| **Dyslipidemia (%)** | 40 | 0.0 | 85.3 † | 20.7 | 13.5 | 26.0 |
| **Aortic Regurgitation Degree (%)** | | | | | | |
| **0** | 69.8* | 100* | 42.1*,† | 15.3 | 17.4 | 13.5 |
| **1** | 20.9 | 0 | 36.8 | 76.5 | 78.3 | 75 |
| **2** | 9.3 | 0 | 21.1 | 8.2 | 4.3 | 11.6 |
| **3** | 0 | 0 | 0 | 0 | 0 | 0 |
| **Aortic Stenosis Degree (%)** | | | | | | |
| **Absent** | 97.7* | 100 | 94.7 | 71 | 80.4 | 63 |
| **Mild** | 0 | 0 | 0 | 18 | 8.7 | 25.9 |
| **Moderate** | 2.3 | 0 | 5.3 | 11 | 10.9 | 11.2 |
| **Severe** | 0 | 0 | 0 | 0 | 0 | 0 |
| **Systolic Arterial Pressure (mm Hg)** | 131.9±19.3 | 135.2±21.7 | 127.1±14.6* | 136.2±15.9 | 133.4±13.7 | 138.3±17.2 |
| **Diastolic Arterial Pressure (mm Hg)** | 67.6±12.6* | 67.7±13.0 * | 67.4±12.3* | 76.8±9.1 | 75.0±8.2 | 78.1±9.6 |
| **SoV Diameter (mm)** | 34.2±7.1* | 31.1±4.5 * | 37.8±7.9† | 36.2±4.6 | 34.3±4.5 | 37.7±4.3† |
| **AscAo Diameter (mm)** | 36.3±11.4* | 29.6±5.9 * | 44.2±11.3† | 41.1±7.6 | 37.4±7.1 | 43.9±6.7† |
| **Proximal arch diameter (mm)** | 29.1±5.6 | 25.2±3.2 | 33.5±4.2† | 30.8±5.5 | 25.8±3.1 | 34.6±3.6† |

*Table 2. Flow dynamics at proximal and distal arch per BAV-phenotype and arch dilation. Statistical significance (p<0.05) is indicated: *RL vs RN-BAV, †compared to dilated RL-BAV.*

| | | RL-BAV | | | RN-BAV | | |
|---|---|---|---|---|---|---|---|
| | | ALL (n=83) | Non-dilated (n=44) | Dilated (n=39) | ALL (n=28) | Non-dilated (n=4) | Dilated (n=24) |
| **Vmax (cm/s)** | **Proximal** | 103.08±29.01 | 99.39±27.48 | 107.23±30.45 | 108.27±33.24 | 100.74±48.04 | 109.53±31.37 |
| | **Distal** | 98.50±24.39 | 99.17±24.57 | 97.75±24.48 | 108.29±47.19 | 97.62±31.03 | 110.07±49.65 |
| **Jet Angle (º)** | **Proximal** | 15.57±7.45 | 14.83±7.58 | 16.40±7.30 | 16.05±6.18 | 13.96±6.76 | 16.40±6.16 |
| | **Distal** | 15.39±6.16 | 15.83±6.47 | 14.89±5.84 | 14.78±8.40 | 20.00±20.13 | 13.92±4.94 |
| **Norm Disp** | **Proximal** | 0.07±0.03 | 0.06±0.03† | 0.08±0.03 | 0.07±0.02 | 0.05±0.02 | 0.07±0.02 |
| | **Distal** | 0.06±0.02 | 0.05±0.02 | 0.06±0.02 | 0.06±0.02 | 0.05±0.01 | 0.06±0.02 |
| **IRF ($cm^2/s$)** | **Proximal** | 54.73±45.17* | 44.13±34.20† | 66.69±52.95 | 122.53±103.97 | 53.32±58.97 | 134.07±106.14† |
| | **Distal** | 16.19±15.88* | 12.85±14.89† | 19.96±16.31 | 31.50±40.66 | 21.39±19.60 | 33.18±43.25 |
| **SFRR (%)** | **Proximal** | 13.52±11.92 | 8.58±8.90† | 19.09±12.53 | 13.85±7.10 | 9.95±2.65 | 14.50±7.43 |
| | **Distal** | 6.21±6.59 | 4.43±4.95† | 8.22±7.62 | 7.15±5.02 | 4.91±3.33 | 7.53±5.20 |
| **$WSS_{ax,avg}$ ($N/m^2$)** | **Proximal** | 0.27±0.16 | 0.32±0.16† | 0.21±0.15 | 0.24±0.12 | 0.19±0.05 | 0.25±0.12 |
| | **Distal** | 0.41±0.22 | 0.46±0.22† | 0.36±0.22 | 0.35±0.22 | 0.23±0.07 | 0.37±0.23 |
| **$WSS_{circ,avg}$ ($N/m^2$)** | **Proximal** | 0.09±0.07* | 0.08±0.06 | 0.09±0.07 | 0.18±0.15 | 0.07±0.08 | 0.19±0.15† |
| | **Distal** | 0.04±0.04 | 0.03±0.04 | 0.04±0.03 | 0.06±0.09 | 0.03±0.04 | 0.07±0.09 |

*Table 3. Flow dynamics at proximal and distal aortic arch in BAV and TAV per arch dilation. Statistical significance (p<0.05) comparing: *TAV vs BAV counterpart, †dilated vs non-dilated counterpart.*

| | | TAV | | | BAV | | |
|---|---|---|---|---|---|---|---|
| | | ALL (n=45) | Healthy (n=24) | Dilated (n=21) | ALL (n=111) | Non-dilated (n=48) | Dilated (n=63) |
| **Vmax (cm/s)** | **Proximal** | 106.58±37.53 | 110.98±31.70 | 101.55±43.52 | 104.38±30.06 | 99.50±28.96 | 108.11±30.57 |
| | **Distal** | 103.40±36.35 | 107.56±32.75 | 98.63±40.36 | 100.97±31.75 | 99.04±24.78 | 102.44±36.31 |
| **Jet Angle (º)** | **Proximal** | 13.87±4.97 | 14.16±4.65 | 13.55±5.42 | 15.69±7.13 | 14.76±7.45 | 16.40±6.84 |
| | **Distal** | 13.48±4.70 | 14.01±4.58 | 12.87±4.87 | 15.24±6.76 | 16.18±8.10 | 14.52±5.50 |
| **Norm Disp** | **Proximal** | 0.05±0.02* | 0.05±0.02* | 0.04±0.01* | 0.07±0.03 | 0.06±0.03 | 0.07±0.03† |
| | **Distal** | 0.04±0.01* | 0.04±0.02* | 0.04±0.01 | 0.06±0.02 | 0.05±0.02 | 0.06±0.02 |
| **IRF ($cm^2/s$)** | **Proximal** | 30.04±34.93* | 28.28±27.92* | 32.04±42.19* | 71.83±71.06 | 44.90±36.04 | 92.36±83.58† |
| | **Distal** | 22.03±25.26 | 20.58±20.12 | 23.69±30.53 | 20.05±25.27 | 13.56±15.26 | 25.00±25.27† |
| **SFRR (%)** | **Proximal** | 10.50±10.98 | 6.91±8.73 | 14.60±12.03† | 13.60±10.88 | 8.69±8.55 | 17.34±11.04† |
| | **Distal** | 5.42±4.70 | 4.60±4.09 | 6.36±5.26 | 6.45±6.22 | 4.47±4.81 | 7.96±6.77† |
| **$WSS_{ax,avg}$ ($N/m^2$)** | **Proximal** | 0.31±0.19 | 0.38±0.18 | 0.22±0.18† | 0.26±0.15 | 0.31±0.16 | 0.23±0.14† |
| | **Distal** | 0.37±0.20 | 0.43±0.20 | 0.29±0.18† | 0.40±0.22 | 0.44±0.22 | 0.36±0.22 |
| **$WSS_{circ,avg}$ ($N/m^2$)** | **Proximal** | 0.05±0.07* | 0.05±0.05 | 0.05±0.08* | 0.11±0.10 | 0.08±0.06 | 0.13±0.12† |
| | **Distal** | 0.05±0.05 | 0.05±0.04 | 0.05±0.06 | 0.04±0.06 | 0.03±0.04 | 0.05±0.06 |

*Table 4. Unadjusted and adjusted relationship of demographic and local flow variables to proximal arch dilation.*

| | **Unadjusted correlates of arch dilation** | **Multivariable adjusted correlates of arch dilation** | | |
|---|---|---|---|---|
| | **P-value** | **OR** | **95% CI** | **P-value** |
| **Sex (Male)** | 0.007 | 2.57 | 0.61-10.83 | 0.198 |
| **height (cm)** | 0.001 | 1.11 | 1.045- 1.182 | 0.001 |
| **Weight [Kg]** | <0.001 | 1.02 | 0.97-1.07 | 0.520 |
| **DBP [mmHg]** | 0.081 | 1.04 | 0.98-1.10 | 0.148 |
| **SBP [mmHg]** | 0.108 | 1.01 | 0.98-1.04 | 0.723 |
| **BAV-phenotype (RN vs RL)** | <0.001 | 0.254 | 0.062-0.99 | 0.049 |
| **IRF ($cm^2/s$)** | <0.001 | 1.014 | 1.002-1.027 | 0.023 |
| **SFRR (%)** | <0.001 | 1.14 | 1.06-1.22 | <0.001 |

*Table 5. Unadjusted and adjusted relationship of demographic and local flow variables to proximal arch diameter.*

| | **Unadjusted correlates of arch diameter** | **Multivariable adjusted correlates of arch diameter** | |
|---|---|---|---|
| | **P-value** | **95% CI** | **P-value** |
| **Age [years]** | 0.001 | 0.06 – 0.19 | <0.001 |
| **Sex (Male)** | 0.014 | -1.69 – 2.20 | 0.796 |
| **height (cm)** | 0.002 | 0.10 – 0.26 | <0.001 |
| **Weight [Kg]** | <0.001 | -0.09 – 0.07 | 0.836 |
| **DBP [mmHg]** | 0.053 | 0.01 – 0.18 | 0.020 |
| **SBP [mmHg]** | 0.030 | -0.09 – 0.03 | 0.285 |
| **BAV-phenotype (RN vs RL)** | 0.001 | 0.99 – 4.64 | 0.003 |
| **IRF ($cm^2/s$)** | 0.013 | 0.00 – 0.03 | 0.028 |
| **SFRR (%)** | <0.001 | 0.15 – 0.29 | <0.001 |

# Figure legends

**Figure 1.** Regional WSS measurement regions. A: anterior, L: left, P: Posterior, R: right.

**Figure 2.** Normalized displacement and in-plane rotational flow in BAV per BAV phenotype (a, b) and arch dilation (c, d).

**Figure 3.** . Regional WSS maps in the different BAV phenotypes and statistically- significant difference ($p<0.05$). A) Axial WSS shows minimum differences. B) Circumferential WSS is higher in RN-BAV at mid-distal ascending aorta and proximal-mid arch.

**Figure 4.** Flow displacement at the distal ascending aorta and aortic arch in a healthy volunteer and in BAV with non-dilated and dilated arch. Dilated BAV presents increased displacement.

**Figure 5.** Regional WSS maps in BAV patients with dilated and non-dilated arch and statistically-significant difference ($p<0.05$). A) Axial WSS is regionally reduced in presence of dilation. B) Circumferential WSS is increased in dilated BAV in anterior wall at proximal-mid arch.

**Figure 6.** Mean flow parameters along the thoracic aorta in healthy volunteers and BAV with non-dilated and dilated arch, showing differences in the ascending aorta and the proximal arch. Dilated BAV presented higher displacement, systolic flow reversal ratio and contour-averaged WSS than non-dilated, but reduced axial WSS.

# Supplementary material

**Table S1.** Flow dynamics along the aortic arch (proximal to distal slices) in bicuspid aortic valve phenotypes per arch dilation. Statistical significance ($p<0.05$) is indicated: * RL-BAV vs RN-BAV, † compared to dilated RL-BAV.

| | | RL-BAV | | | RN-BAV | | |
|---|---|---|---|---|---|---|---|
| | **Arch slices** | **ALL (n=83)** | **Non-dilated (n=44)** | **Dilated (n=39)** | **ALL (n=28)** | **Non-dilated (n=4)** | **Dilated (n=24)** |
| **Vmax (cm/s)** | **Prox** | 103.08±29.01 | 99.39±27.48 | 107.23±30.45 | 108.27±33.24 | 100.74±48.04 | 109.53±31.37 |
| | **Mid-prox** | 101.19±27.65 | 100.89±28.23 | 101.13±27.34 | 106.19±37.94 | 92.21±28.72 | 108.52±39.27 |
| | **Mid-dist** | 100.10±27.17 | 100.77±29.70 | 99.35±24.36 | 107.85±45.95 | 94.00±35.84 | 110.16±47.67 |
| | **Dist** | 98.50±24.39 | 99.17±24.57 | 97.75±24.48 | 108.29±47.19 | 97.62±31.03 | 110.07±49.65 |
| **Jet Angle (º)** | **Prox** | 15.57±7.45 | 14.83±7.58 | 16.40±7.30 | 16.05±6.18 | 13.96±6.76 | 16.40±6.16 |
| | **Mid-prox** | 14.87±6.62 | 14.23±7.13 | 15.59±6.00 | 15.81±5.61 | 15.60±5.85 | 15.85±5.69 |
| | **Mid-dist** | 13.46±5.26 | 13.08±5.45 | 13.89±5.07 | 14.93±5.96 | 21.69±10.23 | 13.80±4.34 |
| | **Dist** | 15.39±6.16 | 15.83±6.47 | 14.89±5.84 | 14.78±8.40 | 20.00±20.13 | 13.92±4.94 |
| **Norm Disp** | **Prox** | 0.07±0.03 | 0.06±0.03 † | 0.08±0.03 | 0.07±0.02 | 0.05±0.02 | 0.07±0.02 |
| | **Mid-prox** | 0.07±0.03 | 0.06±0.02 | 0.07±0.03 | 0.06±0.02 | 0.07±0.02 | 0.06±0.02 |
| | **Mid-dist** | 0.05±0.02 | 0.05±0.02 | 0.06±0.02 | 0.06±0.02 | 0.05±0.01 | 0.06±0.02 |
| | **Dist** | 0.06±0.02 | 0.05±0.02 | 0.06±0.02 | 0.06±0.02 | 0.05±0.01 | 0.06±0.02 |
| **IRF ($cm^2/s$)** | **Prox** | 54.73±45.17 * | 44.13±34.20 † | 66.69±52.95 | 122.53±103.97 | 53.32±58.97 | 134.07±106.14 † |
| | **Mid-prox** | 38.55±31.24 * | 32.50±23.73 † | 45.38±37.12 | 84.05±71.55 | 49.40±55.62 | 89.83±73.23 † |
| | **Mid-dist** | 24.09±21.69 * | 19.96±16.91 † | 28.75±25.48 | 51.04±52.25 | 37.92±44.56 | 53.23±53.95 † |
| | **Dist** | 16.19±15.88 * | 12.85±14.89 † | 19.96±16.31 | 31.50±40.66 | 21.39±19.60 | 33.18±43.25 |
| **SFRR (%)** | **Prox** | 13.52±11.92 | 8.58±8.90 † | 19.09±12.53 | 13.85±7.10 | 9.95±2.65 | 14.50±7.43 |
| | **Mid-prox** | 10.89±10.11 | 6.97±6.82 † | 15.31±11.40 | 11.94±6.44 | 5.92±12.95 | 12.95±6.35 |
| | **Mid-dist** | 7.74±7.42 | 5.59±5.86 † | 10.15±8.27 | 9.56±5.70 | 6.10±2.91 | 10.13±5.89 |
| | **Dist** | 6.21±6.59 | 4.43±4.95 † | 8.22±7.62 | 7.15±5.02 | 4.91±3.33 | 7.53±5.20 |
| **WSSmag,avg ($N/m^2$)** | **Prox** | 0.38±0.16 | 0.42±0.15 † | 0.35±0.16 | 0.39±0.18 | 0.28±0.07 | 0.41±0.19 |
| | **Mid-prox** | 0.42±0.21 | 0.47±0.21 † | 0.37±0.19 | 0.37±0.17 | 0.31±0.16 | 0.38±0.16 |
| | **Mid-dist** | 0.46±0.25 | 0.52±0.27 † | 0.39±0.21 | 0.39±0.25 | 0.28±0.07 | 0.40±0.27 |
| | **Dist** | 0.48±0.22 | 0.52±0.22 | 0.43±0.21 | 0.45±0.23 | 0.30±0.06 | 0.47±0.24 |
| **WSSax,avg ($N/m^2$)** | **Prox** | 0.27±0.16 | 0.32±0.16 † | 0.21±0.15 | 0.24±0.12 | 0.19±0.05 | 0.25±0.12 |
| | **Mid-prox** | 0.32±0.20 | 0.38±0.20 † | 0.25±0.19 | 0.23±0.13 | 0.22±0.13 | 0.24±0.13 |
| | **Mid-dist** | 0.37±0.25 | 0.44±0.27 † | 0.30±0.20 | 0.27±0.23 | 0.19±0.07 | 0.28±0.24 |
| | **Dist** | 0.41±0.22 | 0.46±0.22 † | 0.36±0.22 | 0.35±0.22 | 0.23±0.07 | 0.37±0.23 |
| **WSScirc,avg ($N/m^2$)** | **Prox** | 0.09±0.07 * | 0.08±0.06 | 0.09±0.07 | 0.18±0.15 | 0.07±0.08 | 0.19±0.15 † |
| | **Mid-prox** | 0.08±0.06 * | 0.07±0.06 | 0.08±0.06 | 0.13±0.11 | 0.09±0.13 | 0.13±0.10 † |
| | **Mid-dist** | 0.05±0.05 * | 0.04±0.05 | 0.05±0.04 | 0.09±0.11 | 0.07±0.08 | 0.09±0.11 † |
| | **Dist** | 0.04±0.04 | 0.03±0.04 | 0.04±0.03 | 0.06±0.09 | 0.03±0.04 | 0.07±0.09 |

**Table S2.** Flow dynamics along the aortic arch (proximal to distal slices) in bicuspid aortic valve and age-matched tricuspid valve subjects per arch dilation. Statistical significance ($p<0.05$) is indicated: * TAV vs BAV, † comparing dilated vs non-dilated counterpart.

| | | TAV | | | BAV per arch dilation | | |
|---|---|---|---|---|---|---|---|
| | **Arch slices** | **ALL (n=45)** | **Healthy (n=24)** | **Dilated (n=21)** | **ALL (n=111)** | **Non-dilated (n=48)** | **Dilated (n=63)** |
| **Vmax (cm/s)** | **Prox** | 106.58±37.53 | 110.98±31.70 | 101.55±43.52 | 104.38±30.06 | 99.50±28.96 | 108.11±30.57 |
| | **Mid-prox** | 108.03±36.27 | 113.28±30.78 | 102.02±41.64 | 102.31±30.47 | 100.17±28.07 | 103.94±32.30 |
| | **Mid-dist** | 106.71±37.44 | 109.73±32.28 | 103.25±43.15 | 102.06±32.86 | 100.21±29.88 | 103.47±35.14 |
| | **Dist** | 103.40±36.35 | 107.56±32.75 | 98.63±40.36 | 100.97±31.75 | 99.04±24.78 | 102.44±36.31 |
| **Jet Angle (º)** | **Prox** | 13.87±4.97 | 14.16±4.65 | 13.55±5.42 | 15.69±7.13 | 14.76±7.45 | 16.40±6.84 |
| | **Mid-prox** | 13.69±5.03 | 14.07±4.92 | 13.25±5.23 | 15.11±6.37 | 14.34±6.99 | 15.69±5.84 |
| | **Mid-dist** | 14.82±5.98 | 15.83±5.08 | 13.66±6.81 | 13.83±5.45 | 13.80±6.30 | 13.86±4.77 |
| | **Dist** | 13.48±4.70 | 14.01±4.58 | 12.87±4.87 | 15.24±6.76 | 16.18±8.10 | 14.52±5.50 |
| **Norm Disp** | **Prox** | 0.05±0.02 * | 0.05±0.02 * | 0.04±0.01 * | 0.07±0.03 | 0.06±0.03 | 0.07±0.03 † |
| | **Mid-prox** | 0.05±0.01 * | 0.05±0.01 * | 0.05±0.02 * | 0.07±0.03 | 0.06±0.02 | 0.07±0.03 † |
| | **Mid-dist** | 0.05±0.02 | 0.05±0.02 | 0.05±0.01 * | 0.06±0.02 | 0.05±0.02 | 0.06±0.02 |
| | **Dist** | 0.04±0.01 * | 0.04±0.02 * | 0.04±0.01 | 0.06±0.02 | 0.05±0.02 | 0.06±0.02 |
| **IRF ($cm^2/s$)** | **Prox** | 30.04±34.93 * | 28.28±27.92 * | 32.04±42.19 * | 71.83±71.06 | 44.90±36.04 | 92.36±83.58 † |
| | **Mid-prox** | 30.07±35.08 * | 27.58±27.05 | 32.92±43.00 * | 50.03±48.77 | 33.91±27.11 | 62.31±57.51 † |
| | **Mid-dist** | 27.24±33.61 | 25.13±28.48 | 29.65±39.26 | 30.89±34.04 | 21.46±20.33 | 38.08±40.27 † |
| | **Dist** | 22.03±25.26 | 20.58±20.12 | 23.69±30.53 | 20.05±25.27 | 13.56±15.26 | 25.00±25.27 † |
| **SFRR (%)** | **Prox** | 10.50±10.98 | 6.91±8.73 | 14.60±12.03 † | 13.60±10.88 | 8.69±8.55 | 17.34±11.04 † |
| | **Mid-prox** | 8.76±8.29 | 6.18±7.07 | 11.70±8.76 † | 11.16±9.30 | 6.88±6.57 | 14.41±9.79 † |
| | **Mid-dist** | 7.06±5.80 | 5.29±4.64 | 9.09±6.41 † | 8.20±7.04 | 5.64±5.66 | 10.15±7.40 † |
| | **Dist** | 5.42±4.70 | 4.60±4.09 | 6.36±5.26 | 6.45±6.22 | 4.47±4.81 | 7.96±6.77 † |
| **WSSmag,avg ($N/m^2$)** | **Prox** | 0.39±0.21 | 0.46±0.18 | 0.31±0.21 † | 0.39±0.17 | 0.40±0.15 | 0.37±0.18 |
| | **Mid-prox** | 0.39±0.21 | 0.48±0.20 | 0.30±0.18 † | 0.41±0.20 | 0.45±0.21 | 0.37±0.19 † |
| | **Mid-dist** | 0.42±0.21 | 0.49±0.21 | 0.34±0.17 † | 0.44±0.25 | 0.50±0.27 | 0.39±0.23 † |
| | **Dist** | 0.43±0.20 | 0.50±0.20 | 0.35±0.19 † | 0.47±0.22 | 0.50±0.22 | 0.45±0.22 |
| **WSSax,avg ($N/m^2$)** | **Prox** | 0.31±0.19 | 0.38±0.18 | 0.22±0.18 † | 0.26±0.15 | 0.31±0.16 | 0.23±0.14 † |
| | **Mid-prox** | 0.31±0.20 | 0.40±0.20 | 0.21±0.15 † | 0.30±0.19 | 0.36±0.20 | 0.25±0.17 † |
| | **Mid-dist** | 0.34±0.20 | 0.42±0.21 | 0.26±0.16 † | 0.35±0.25 | 0.42±0.27 | 0.29±0.22 |
| | **Dist** | 0.37±0.20 | 0.43±0.20 | 0.29±0.18 † | 0.40±0.22 | 0.44±0.22 | 0.36±0.22 |
| **WSScirc,avg ($N/m^2$)** | **Prox** | 0.05±0.07 * | 0.05±0.05 | 0.05±0.08 * | 0.11±0.10 | 0.08±0.06 | 0.13±0.12 † |
| | **Mid-prox** | 0.06±0.07 * | 0.06±0.06 | 0.06±0.08 * | 0.09±0.08 | 0.07±0.06 | 0.10±0.09 |
| | **Mid-dist** | 0.06±0.07 | 0.06±0.08 | 0.05±0.07 | 0.06±0.07 | 0.05±0.05 | 0.07±0.08 |
| | **Dist** | 0.05±0.05 | 0.05±0.04 | 0.05±0.06 | 0.04±0.06 | 0.03±0.04 | 0.05±0.06 |